JOURNAL OF MATERIALS SCIENCE **34** (1999) 5081–5088

Physico-chemical characterisation of native air-formed oxide films on Al-Mg alloys at low temperature. Influence of water

S. SCOTTO-SHERIFF, E. DARQUE-CERETTI
ENSMP—CEMEF, UMR 7635, B.P. 207, 06904 Sophia-Antipolis Cedex, France

G. PLASSART, M. AUCOUTURIER
Lab. Métallurgie Structurale, URA CNRS 1107, Bât. 410, Université Paris-Sud, 91405 Orsay Cedex, France

Natural oxide films on two cold-rolled Al-Mg alloys were studied using several techniques (XPS, SIMS, ToF-SIMS, GDOS, SEM, TEM, Wetting measurements). The aim was to characterise and compare the oxide layers formed on the two materials in order to better understand the influence of the thermomechanical history. The experimental tools used allowed the determination of the influence of the annealing process on the nature and structure of the oxides. The hydration and Brönsted behaviour were also investigated. The thickness of the layer, the amount of magnesium oxide and its dissolving resistance in water are strongly modified by the annealing. The oxide film formed on the annealed material is twice as thick as the one on the non-reheated material. The layer on the annealed material contains more magnesium oxide and contains the crystalline forms: β-Al_2O_3 and bayerite ($Al(OH)_3$). On the contrary, the oxide film formed on the as-rolled material seems to be amorphous. The magnesium oxide is less soluble in water in the annealed film than in the non-reheated one. Furthermore, aluminium and magnesium oxides were found to be hydroxylated on both alloys, and the layer surfaces to behave like a Brönsted meaning base.

1. Introduction

The 5000 series Al-Mg alloy sheets are used for a wide variety of industrial applications such as automobile body panels, conditioning, and acoustic devices. A large number of investigations have been conducted on surface analysis of polished and re-oxidised aluminium and aluminium alloys, since several decades. One may for instance quote a quite ancient work on aluminium-magnesium alloys [1]. Some information on the pioneer modern surface investigations may be found in reference [2], but the existence of several more recent publications (see for instance references [3–6]) proves that the structure and composition of that kind of film is still under discussion. The oxides investigated in those studies are grown in laboratory conditions and may be considered as model films, but very few papers deal with natural oxides formed on rough surfaces, in actual industrial conditions. The present paper is especially interested in the layer grown during working of Al-Mg alloy sheets.

Studies about cold-rolling and adhesive bonding were carried out on two different alloys, as-rolled A5182 (Al-4.7 wt% Mg) and annealed A5086 (Al-4 wt% Mg), respectively. It is interesting to point out that the chemical compositions of the two substrates are close. The main difference is the annealing undergone by the A5086 sheet.

For the as-rolled alloy, the study aimed at understanding the influence of the working process on the nature and behaviour of the oxide and underlying metal. In the case of the annealed alloy, the knowledge of the layer was essential for understanding adhesive bond strength. Indeed, the microscopic morphology and chemistry are important in determining bondability. The purpose of this paper is to investigate the effects of the annealing stage on composition, structure, water reactivity and the acid-base properties of the natural oxide film formed on the alloys. Several microscopic and spectroscopic techniques were used on as-received and hydrated samples.

2. Experimental

2.1. Materials and specimen preparation

Two commercial cold-rolled alloys were used in this study. The ingots were pre-heated at 500 °C, then hot-rolled between 500 and 300 °C, and finally cold-rolled. The as-rolled sheets were 0.6 mm thick with a roughness of 0.35 μm (r_{max} measured by mechanical microprofilometry). The annealed sheets were 1 mm thick with a roughness of 0.25 μm. They were annealed at 360 °C during 12 h in air. The composition of the alloys is given in Table I. The samples were cut to appropriate size depending on the used technique. All samples used in the study were degreased, by the following procedure: The as-rolled samples were ultrasonically cleaned

TABLE I Composition of alloys A5182 and A5086 (wt %)

Alloy	Mg	Mn	Fe	Si	Cu	Cr	Zn	Ti
A5182 (as-rolled)	4.70	0.37	0.24	0.10	0.06	0.0015	0.006	0
A5086 (annealed)	4.00	0.22	0.38	0.20	0.03	0.15	0.03	0.01

in hexane during 5 min. The annealed samples were degreased in a trichloroethylene vapour bath during 5 min. The reaction between the oxide layer and water was also investigated by dipping the samples into boiling deionized water for 90 s.

2.2. Techniques

Scanning electron images (SEM) were obtained with a CAMBRIDGE INSTRUMENT microscope or with a JEOL microscope. Both microscopes were equipped with an energy dispersive X-ray spectroscopy (EDS) system. These techniques were used to study the topographical and chemical aspect of the surface.

A JEOL 2000 EX transmission electron microscope (TEM) was used to image the oxide layer of the as-rolled alloy. The samples were ultramicrotomed cross sections.

The surface crystallinity of the oxides was investigated by low angle electron diffraction, in a PHILIPS CM 12 TEM.

The surface composition of the oxide layers before and after hydration was investigated by X-ray induced photoelectron spectroscopy (XPS). Spectra were recorded with two different spectrometers. The first one was a LEYBOLD equipped with an AlK_α (1486.6 eV) source, and a manipulator which allows the rotation of the sample with respect to the analyser axis (angle-resolved XPS: θ is the angle between the surface and the detection direction). The second spectrometer was a RIBER. The source was a MgK_α (1253.6 eV) radiation. The pressure inside the spectrometer chamber was around 10^{-7} Pa and the source power was near 250 W. The sample size was 12×15 mm^2. Some sputter etching was carried out at approximately $3 \cdot 10^{-4}$ Pa with an argon ion beam. Both spectrometer display an in-situ heating specimen holder, used for analyses after heating under high vacuum.

Secondary ion mass spectroscopy (SIMS) profiles were recorded with a CAMECA IMS3f analyser. The samples were sputtered with a primary ion beam of $^{40}Ar^+$. The diameter of the analysed area was 60 μm. The incident angle of the primary beam (still referred to the surface) for 5.5 keV primary sputtering energy and positive secondary ion detection was 48°. The sputtering current density was 5 $\mu A \cdot cm^{-2}$. Those conditions were chosen to minimise the effect of the primary beam implantation transitory stage.

Static SIMS was performed in a Time-of-Flight spectrometer (ToF-SIMS, CHARLES EVANS and ASSOCIATES). The samples were bombarded with a primary ion beam of $^{115}In^+$ (15 keV). The analysed area was 120 μm in diameter. Positive secondary ions were analysed. The Glow-Discharge Optical Spectrometry (GDOS) measurements were made on a LECO 1000, which allowed ionic erosion with a current of 50 mA and a voltage of 500 V. The diameter of the sputtered area was 4 mm.

The acid and basic properties were estimated through the drop contact angle titration method at room temperature (20 °C). Contact angles of pH buffered solutions were measured on a KRÜSS contact angle measuring system to detect surface ionizable functionality in a qualitative manner. Constant volume droplets of 0.5 μl were delivered. On every sample at least ten measurements were performed; the scattering from the average value was no more than 2°.

3. Experimental results and discussion

3.1. As-received state

3.1.1. Microscopy results

A SEM image of the surface of as-received alloys A5182 and A5086, after cleaning, is shown in Fig. 1. Rolling stripes are observed and the matrix is partly covered with bright and dark particles. Using EDS, the bright particles are identified as (Al, Fe, Mn)-containing intermetallic compounds. The dark ones are enriched in carbon and oxygen. The oxide layer may be thicker in these areas. Another explanation can be the existence of hydroxides. Examination of the surface exhibits the presence of cracks, revealing the metal substrate. SEM analyses display a non-homogeneous oxide film. TEM investigations (Fig. 2) also show that the oxide thickness is irregular.

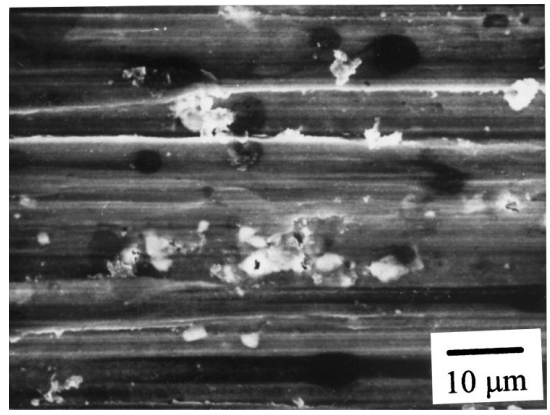

Figure 1 SEM image representative of the surface of both alloys after cleaning.

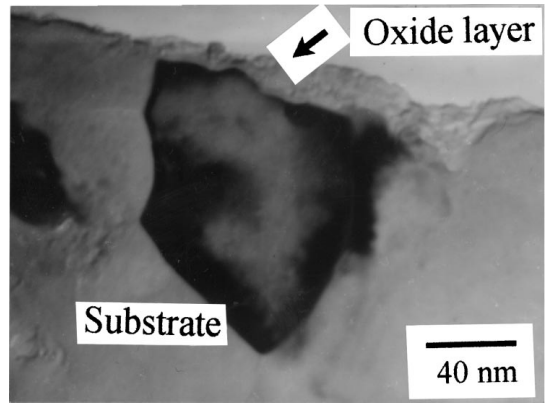

Figure 2 TEM image of an ultramicrotomed cross-section on the as-rolled alloy.

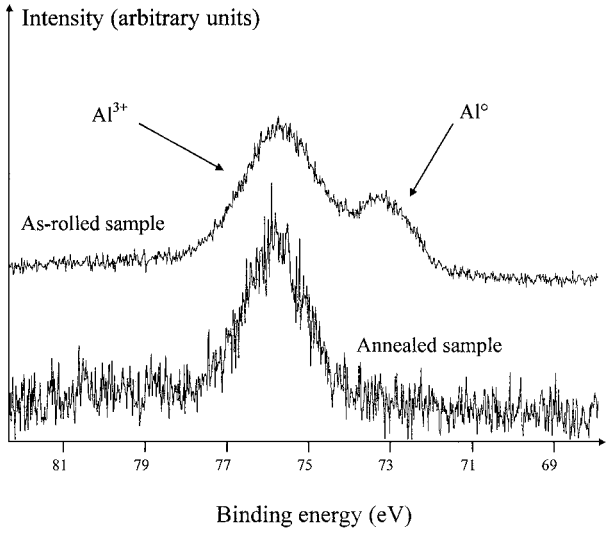

Figure 3 XPS: comparison of Al2p spectra for both alloys at $\theta = 90°$. Intensity scales are different.

3.1.2. Composition and microstructure

The chemical composition of the oxides was investigated using XPS, SIMS and ToF-SIMS. TEM was used to characterise the microstructure.

For each sample, core-level spectra in the C1s, Al2p, Mg2p and O1s regions were recorded by XPS.

The C1s emission is certainly due to a variety of adsorbed hydrocarbons and a minor peak at higher binding energy can be attributed to carbonate and organic carboxylate groups [7].

The Al2p envelope exhibits two peaks. The low binding energy component can be attributed to metallic aluminium, mostly issued from the substrate, and the higher binding energy line can be associated with the aluminium oxides and hydroxides [8–11]. Fig. 3 shows the spectra of the Al2p core-level obtained for the two alloys. These curves indicate that the thickness of the oxide film is larger on the annealed sample.

The Mg2p region consists of an oxidised peak with a low binding energy shoulder which could be assigned to $Mg(OH)_2$ [10–13]. Indeed, it was verified that when a Mg oxide grown on pure magnesium substrate is hydrated in boiling water for 10 min, the Mg2p peak shifts towards low binding energies.

The atomic ratio between the elements Mg and Al in the oxidised state, estimated using the photoelectric cross-sections calculated by Scofield [14], varies from 1 for the as-rolled sample to 1.8 for the annealed one. Then, the annealing undergone by the A5086 sheet has resulted in a larger concentration of Mg^{2+} in the oxide film. This phenomenon is reported by several authors [5, 8, 15].

It is worth underlying that there is a substantial Mg enrichment in the outermost layers of the alloys where $Mg/Al = 1$ to 2, compared to the bulk atomic ratio of 0.05.

The oxide film thickness can be estimated using the following equation, based upon Seah and Dench relation [10],

$$d_{oxide} = \lambda_{oxide} \times \ln[(I_{oxide} \times \lambda_{metal})/(I_{metal} \times N_{oxide} \times \lambda_{oxide}) + 1]$$

TABLE II Estimated oxide thickness on as-received alloys A5182 and A5086

Alloy	A5182 as-rolled	A5086 annealed
Oxide thickness (nm)	4	7

- λ_{oxide} is the mean free path of photoelectrons in the oxide layer, estimated from the calculated free paths in Al_2O_3 and MgO [10] and balanced by the respective amount of the oxidised Al2p and Mg2p components.
- λ_{metal} is the mean free path of photoelectrons in the substrate.
- I_{oxide} is the percentage of the summed Al2p and Mg2p oxide peaks areas in the spectrum, taking into account the cross section for each peak.
- I_{metal} is the percentage of Al2p metallic aluminium component in the spectrum.
- N_{oxide} is the average atomic ratio of Al and Mg in the duplex Al_2O_3/MgO oxide.

The calculation gives estimated average thickness because the substrate roughness, the non-homogeneity of the oxide layer, and the existence of hydroxides are not taken into account in the above equation. The obtained values are given in Table II, and verify the assumption that the thickness is larger on the annealed sample than on the as-rolled one, as illustrated by Fig. 3.

Considering the O1s core-level, the recorded spectra are wide, indicating the presence of a mixture of more or less hydrated or hydroxylated Al and Mg oxides. On both O1s peaks, a shoulder is detected on the low binding energy side. This component can be related to $Mg(OH)_2$, as it was determined on the Mg2p line.

In order to interpret the different components of the O1s peak, dehydration experiments were performed (300 °C for 3 h in the spectrometer chamber vacuum). From those investigations, the O1s spectrum before dehydration could be interpreted as containing four (as-rolled alloy) or three (annealed alloy) components. In the order of increasing binding energy, the identified components (Fig. 4) are due to the following bonds*: Mg-O-H ($Mg(OH)_2$) at 531.5 eV; Al-O and Mg-O (Al_2O_3 and MgO, not separated) at 532.4 eV; Al-O-H (AlO(OH) or $Al(OH)_3$) plus contamination C-O, at 533.5 eV; H_2O plus contamination C=O, at 534.6 eV. The decomposition of the O1s spectrum on the as-received (Fig. 4a) and dehydrated (Fig. 4b) samples shows an important apparent shift of the peak, associated to narrowing (note that the Al2p and Mg2p peaks are not shifted in these conditions). This confirms that the major component situated at a high binding energy (533.5 eV), quasi-eliminated by heating, can be attributed to aluminium hydroxides (AlO(OH) or $Al(OH)_3$), as in published data [7, 16–19].

The non-occurrence of the peak attributed to H_2O [10, 16, 17] for the alloy 5086 is probably due to desorption of water induced by the annealing process.

* Energy calibration is not corrected, as Al° peak is detected at its normal value (72.9 eV). Background Shirley correction is used. Peaks are fitted with a Lorentzian-Gaussian (L/G = 0.1) model and FWHM = 2 ± 0.2 eV.

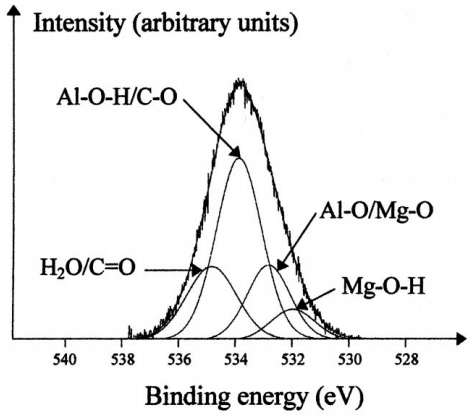

(a)

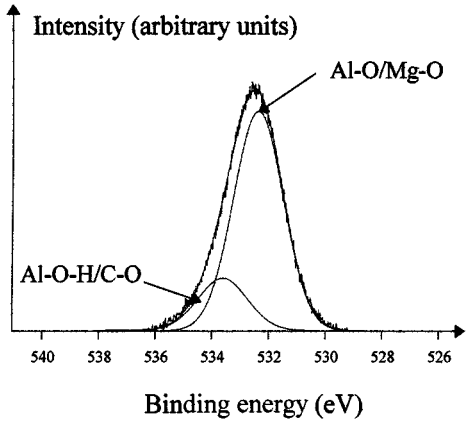

(b)

Figure 4 XPS: O1s peak fitting on the as-rolled alloy: (a) before dehydration (as-received), (b) after dehydration (300 °C, high vacuum).

Further information on the composition and structure of the oxide film is obtained using SIMS, ToF-SIMS and low-angle electron diffraction.

In the SIMS profiles performed on the as-rolled sample, the OH^+ and MgO^+ signals exhibit exactly the same evolution with the sputtering time. Moreover, peak maxima of those signals are obtained at the early stage of the abrasion, which indicates that the upper layer of the oxide film might include Mg hydroxide.

On the annealed sample, ToF-SIMS spectra confirm the presence of Al- and Mg-containing species on the extreme surface.

Concerning the oxide microstructures, the low-angle electron diffraction patterns (Fig. 5) confirm the well-known [2, 20] influence of temperature on their crystallinity. On the annealed sample the oxide microstructure is partially crystallised, and exhibit β-Al_2O_3 (11 Al_2O_3.MgO) and bayerite ($Al(OH)_3$) crystal structures (Fig. 5a and b). Lea [15] and Doherty [21] found that amorphous Al_2O_3 films on non-allied aluminium heated above 350–400 °C turn into γ crystalline form. The presence of the β-Al_2O_3 crystalline form, instead of the expected γ form has never been mentioned to our knowledge in that temperature range, and may be attributed to the high magnesium content. No obtained pattern can be associated with MgO, indicating that this oxide is probably amorphous. As some lines of the $Mg(OH)_2$ diagrams are similar to the β-Al_2O_3 diagram, it is not possible to conclude about the crystallinity of the $Mg(OH)_2$ compound. The same experiment performed on the as-rolled alloy does not reveal any diffraction pattern, suggesting, as expected, that oxides are amorphous. This was confirmed by the absence of diffraction contrast in TEM observation of that alloy (Fig. 2).

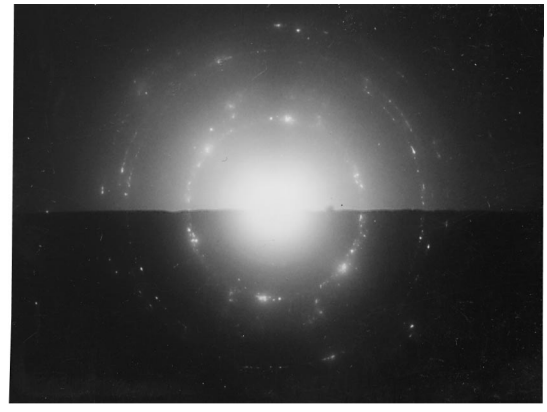

(a)

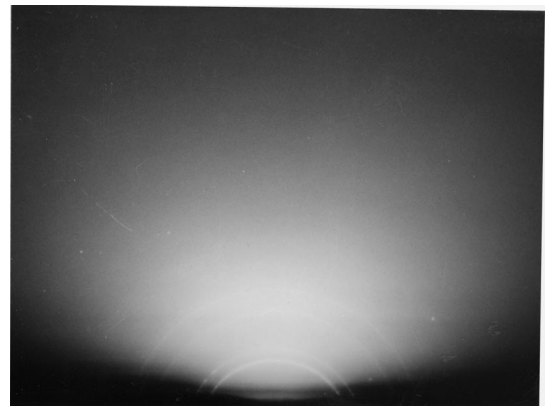

(b)

Figure 5 Low-angle electron diffraction patterns on the annealed alloy: (a) β-Al_2O_3 (11 Al_2O_3.MgO), (b) Bayerite ($Al(OH)_3$).

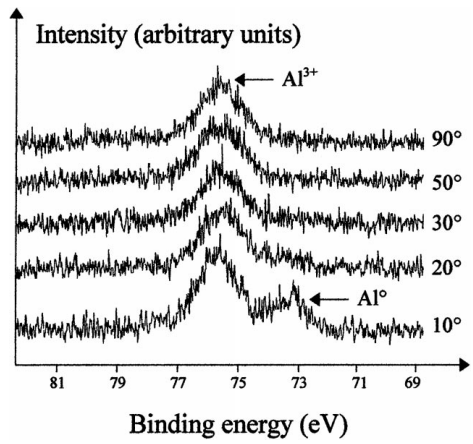

Figure 6 Angle-resolved XPS: Al2p peak variation on the as-received annealed alloy.

Some angle-resolved XPS experiments were carried out on the alloys. As shown on Fig. 6, the metallic component intensity on the Al2p line (annealed sample) is increasing for take-off angles equal or smaller than 20° (referred to the surface). On the as-rolled alloy, the logical decrease of metallic aluminium is observed down to 20°, but below this take-off angle, the importance of the metallic aluminium component increases also.

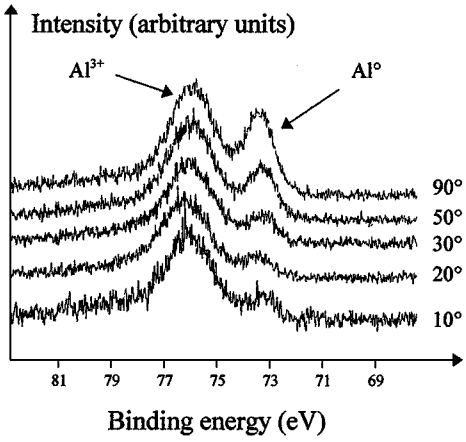

Figure 7 Angle-resolved XPS: Al2p peak variation on an etched annealed sample.

One of the causes for this last phenomenon may be the substrate roughness which can disturb measurements at very low take-off angles. This roughness effect can be ruled out by XPS results obtained on an etched annealed sample (Fig. 7), which exhibits a roughness twice as important as the non-etched sample but presents a logical decrease of the Al2p metallic component when the take-off angle decreases. Note that magnesium is no more detected after etching.

Another reason could be the presence of metallic aluminium in the outermost layers of the oxide film. This last assumption is based on magnesium diffusion through the oxide layer and reduction of Al_2O_3 by Mg^{2+} ions, as follows [7, 22]:

$$Mg + \tfrac{1}{3}Al_2O_3 \rightarrow MgO + \tfrac{2}{3}Al$$

SIMS experiments on the as-rolled sample confirm the presence of metallic aluminium in the oxide layer. Indeed, Al_2^+ signal, which can be considered as representative of the metal state, has a shoulder in the oxide layer (Fig. 8).

The metallic aluminium presence assumption seems to be the most relevant and is also mentioned by several authors [6, 15, 23–25].

3.1.3. Oxide layer organisation

The intensity of the carbonate/carboxylate groups component on C1s XPS spectra is decreasing when take-off angles decrease, suggesting that these compounds are not situated in the upper part of the oxide layer. Note also that the carbonate/carboxylate contribution to the oxide layer could not be eliminated by prolonged polishing.

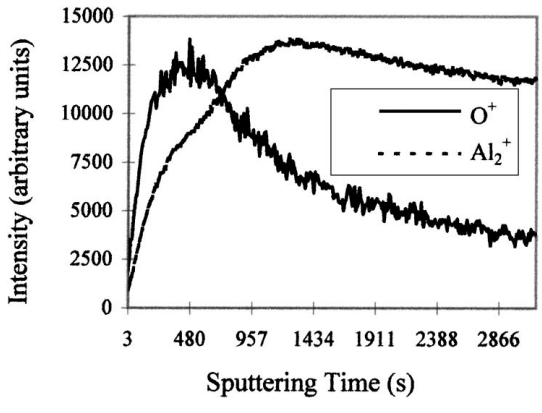

Figure 8 SIMS: Al_2^+ and O^+ profiles on the as-rolled alloy.

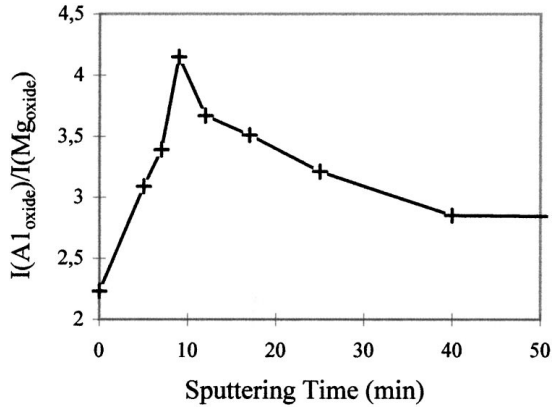

Figure 9 XPS: Al_{oxide}/Mg_{oxide} peak ratio versus sputtering time on the as-rolled alloy.

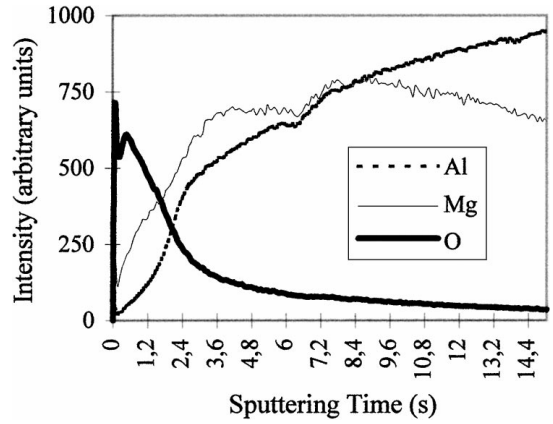

Figure 10 GDOS: O, Mg and Al profiles on the as-rolled alloy.

During argon sputtering, the Al_{oxide}/Mg_{oxide} ratio obtained on the as-rolled alloy from Al2p and Mg2p emissions (Fig. 9) shows a rise in the first stage and then a decrease. This signifies that magnesium is present at the external interface and at the metal/oxide interface. GDOS experiments confirm this magnesium distribution (Fig. 10). A shoulder at the external interface and a maximum at the internal interface are evidenced. SIMS profiles represented on Fig. 11 illustrate the evolution

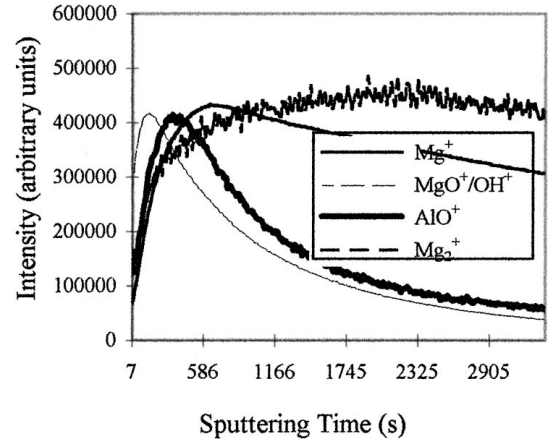

Figure 11 SIMS: OH^+, Mg^+, MgO^+, AlO^+ and Mg_2^+ profiles on as-the rolled alloy (Ar^+ sputtering).

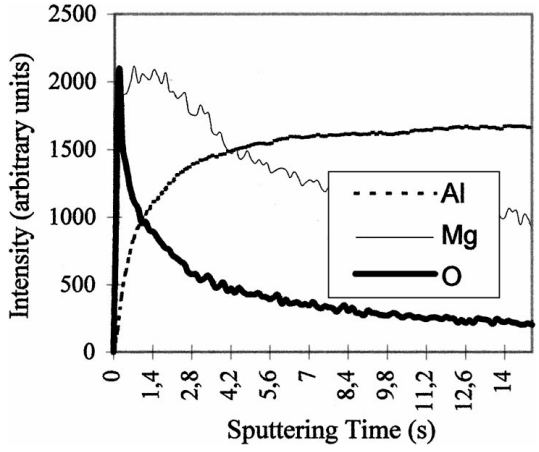

Figure 12 GDOS: O, Mg and Al profiles on the annealed alloy.

of OH^+, Mg^+, MgO^+, AlO^+ and Mg_2^+ signals while sputtering. As explained before, the MgO^+ signal is representative of $Mg(OH)_2$. The Mg^+ signal could be associated with MgO [26] as the metallic state may be characterised by Mg_2^+. The aluminium oxide and hydroxides (AlO^+) seem to be in the layer core, $Mg(OH)_2$ being situated preferentially on the extreme surface and MgO at the internal interface.

GDOS experiments on the annealed sample (Fig. 12) indicate a large magnesium enrichment at the external surface.

For both specimens (Figs 10 and 12), the O signal decreases drastically in the early stage of the sputtering, with a slope change in the core of the film, indicating that the hydroxides (more rich in oxygen) are located in the outer part of the film.

In the oxide layer, the position of MgO is then different between the two alloys. This could be due to the nature of alumina. Indeed, on the annealed sample, a partial crystallisation of Al_2O_3 allows magnesium to diffuse towards the surface using either crystallised alumina grain boundaries or interphase boundaries between the crystalline and amorphous Al_2O_3 as diffusion short-circuits. On the contrary, on the as-rolled alloy, alumina is amorphous and the layer acts as a barrier, which prevents diffusion of a large amount of magnesium through the oxide film [6, 15, 22].

To summarise the composition and microstructure interpretations, a schematic feature of the oxide film organisation for each alloy is proposed in Fig. 13.

3.1.4. Surface acidity/basicity

Fig. 14 illustrates the variation versus pH of the contact angle of different buffered solutions for both alloys. As discussed in a previous work [27], it is important to distinguish between the pH domain of the extreme surface thermodynamical stability, where only 2D interaction occurs with the drop, from the 3D dissolution domains. Here, for $4 \leq pH \leq 9$ the curves are superimposed. Furthermore, measured angles are increasing for pH rising values, which implies a basic character of the surface. This pH interval corresponds to the $Al(OH)_3$ stability domain [16, 27–30].

Below $pH = 4$ and above $pH = 9$, the layer behaviour is different. On the annealed sample, measured contact angle are lower, implying a more significant 3D reaction. The oxide film covering the annealed alloy is then more sensitive to corrosion. This phenomenon is justified by a larger amount of magnesium oxide in the layer which worsen the corroding reaction [31] in those two pH domains.

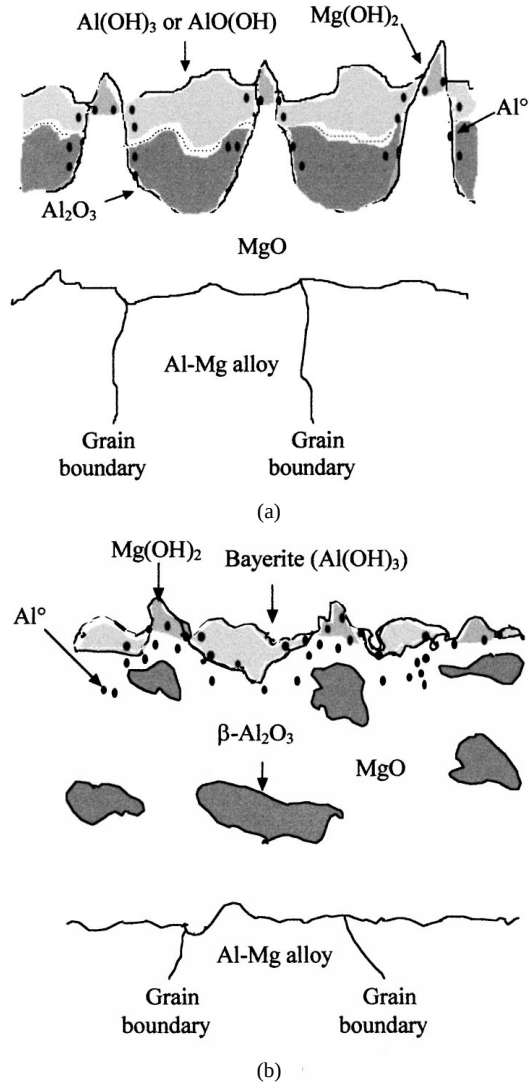

Figure 13 Tentative feature of the oxide films: (a) As-rolled alloy, (b) Annealed alloy.

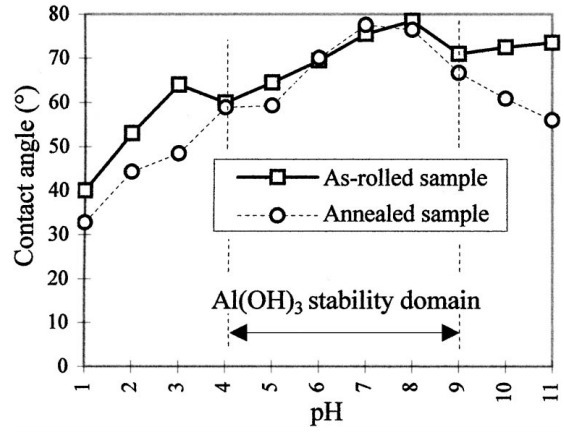

Figure 14 Acidity/basicity contact-angle titration on both alloys.

3.2. Hydrated alloys

Hydrating the as-rolled sample during 90 s leads to pores development and to some cracks around the (Al,

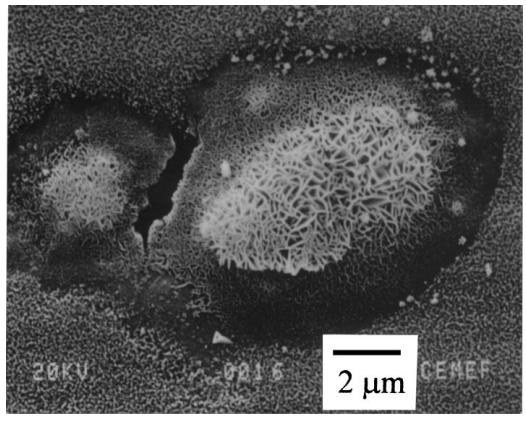

Figure 15 SEM micrograph on the hydrated annealed alloy.

Fe, Mn) intermetallic precipitates. The surface aspect becomes foam-flecked. For the annealed alloy, a significant difference of the surface topography evolution is observed, as compared to the behaviour of the as-rolled sample. This is illustrated by SEM micrography in Fig. 15. Protruding hydrated oxides can be noticed [32–34]. This sub-layer has a dense structure with crack formation.

From low-angle electron diffraction patterns, only $Al(OH)_3$ crystals are found on the hydrated annealed alloy, which may be related to the more numerous protrusions observed by SEM, as compared to the as-rolled alloy. The initial crystalline nature of the annealed film might thus explain the differences between the two hydrated alloys.

Furthermore, magnesium compounds are no more detected by ToF-SIMS at the extreme surface, where only aluminium compounds are present. The combined results of all experiments imply that after hydration, the superficial monolayer of the oxide film is only constituted with aluminium hydroxides.

XPS O1s peak fitting after hydration shows that components attributed to $Mg(OH)_2$ and Al_2O_3/MgO are reduced to the benefit of hydrated aluminium oxides. Al2p and Mg2p spectra also show a decrease of the relative Mg amount in the analysed thickness.

On the annealed sample, a short Ar^+ sputtering restores the Mg2p line as intense as before hydration. On the as-rolled alloy, even a long erosion is ineffective to recover the same Mg quantity as the former oxide film. Magnesium oxide and hydroxide are thus partially dissolved.

The GDOS Mg signal on the as-rolled sample falls down, confirming the partial dissolution of the magnesium oxide. SIMS analysis gives a similar result.

In summary, annealing does not modify the emergence of aluminium hydroxides but influences their morphology and the water dissolving resistance of MgO. This could be due to the magnesium oxide structure and/or amount difference, and to differences in the crystallinity mentioned above.

4. Conclusion

In this physico-chemical and structural study of the native oxide films grown at low temperature on Al-Mg alloys, a comparison between two alloys of similar composition and different thermal history was completed. The thermal history has, in particular, a large influence on the hydration behaviour of the extreme surface film.

The following similarities and differences are evidenced:

- For both alloys, the oxide film is enriched in oxidised Mg, that enrichment being more pronounced for the annealed alloy. The oxide thickness, larger for the annealed alloy, remains less than 10 nm.
- The oxide film contains aluminium in the metallic state, probably as a consequence of the reduction of alumina by diffusing magnesium.
- In both films, aluminium and magnesium hydroxides are present.
- The Brönsted acid-base behaviour of the extreme surface of both oxides is identical and corresponds to the behaviour of $Al(OH)_3$. The higher reactivity of the annealed alloy oxide film for low and high pH is attributed to its higher magnesium content.
- The magnesium distribution is different between the two alloys. Indeed, annealing induces the formation of crystallised alumina, clearly evidenced on those nanometer scaled films by grazing electron diffraction. This may enable a better diffusion of Mg through the film and its oxidation in the outer part of the film formed on the annealed sample, whereas the most part of magnesium is oxidised at the metal/oxide interface on the as-rolled alloy.
- The hydration behaviour of the films is different: Mg oxide and hydroxide are nearly totally dissolved for the as-rolled alloy, but only imbedded for the annealed alloy, for the benefit in both cases of aluminium hydroxides.

Concerning the influence of the observed features on the performances of the native air-grown oxide films in service conditions, the following appreciation may be proposed:

- For adhesive bonding application, both surfaces exhibit the same Brönsted acid-base reactivity, which suggests a similar wetting behaviour. The higher surface reactivity experienced for the annealed alloy would lead to suggest this type of treatment, followed by the surface cleaning described in Section 2.1.
- For the problem of surface behaviour during cold-rolling, this investigation has shown that the presence of magnesium as an alloying element increases drastically the susceptibility to water degradation of the native oxide film, leading to a selective dissolution of the magnesium oxide and the formation of mechanically weak aluminium hydroxide. This should have deleterious consequences on the protecting character of the film, and on the reactions with lubricants within the cold-rolling mill roll-gap.

That comparison of specimens with a complex composition has evidenced the influence of the thermomechanical treatments on the surface film composition and

structure, as well as their behaviour in presence of water. Such conclusions could not have been drawn without the conjunction of several complementary characterisation methods.

Acknowledgements

The authors would like to thank Thomson Marconi Sonar and CPR concluded between CNRS (SCA), IRSID, Pechiney Recherche, Universite Paris-Sud Orsay (LMS), College de France (PMC), ECL (LTDS), Insa de Lyon (LMC) and ENSMP (CEMEF) for their financial supports.

Authors would also like to acknowledge G. Rautureau and E. Beauprez (DGA) for SIMS measurements, L. Kuntzler and G. Boutin (IRSID) for GDOS experiments, M. Roux-Michollet (CRV Pechiney) for ultramicrotomed cross-sections, M. Combarieu (ENSMP-CEMEF) for technical XPS and ToF-SIMS assistance, M. Perrin (ENSMP-CEMEF) for low-angle electron diffraction and A. M. Huntz for discussion.

References

1. L. DE BROUCKERE, *J. Inst. Met*. **71** (1945) 131.
2. J. BENARD, in "L'Oxydation Des Métaux" (Gauthiers-Villars, Paris, 1964) pp. 363–366.
3. A. NYLUND and I. OLEFJORD, *Surf. Interface Anal*. **21** (1994) 283.
4. K. MIZUNO, A. NYLUND and I. OLEFJORD, *Mater. Sci. Technol*. **12** (1996) 306.
5. G. R. WAKEFIELD and R. M. SHARP, *Appl. Surf. Sci*. **51** (1991) 95.
6. T. S. SUN, J. M. CHEN, R. K. VISWANADHAM and J. A. S. GREEN, *J. Vac. Sci. Technol.* **16**(2) (1979) 668.
7. M. TEXTOR and R. GRAUER, *Corros. Sci.* **23**(1) (1983) 41.
8. A. ARRANZ and C. PALACIO, *Surf. Sci.* **355** (1996) 203.
9. T. L. BARR, S. SEAL, L. M. CHEN and C. C. KAO, *Thin Solid Films* **253** (1994) 277.
10. D. BRIGGS and M. P. SEAH, "Auger and X-ray Photoelectron Spectroscopy" (Wiley, Chichester, 1996) pp. 153, 209, 599–602.
11. E. MCCAFFERTY and J. P. WIGHTMAN, *Surf. Interface Anal.* **26** (1998) 549.
12. S. ARDIZZONE, C. L. BIANCHI, M. FADORI and B. VERCELLI, *Appl. Surf. Sci*. **119** (1997) 253.
13. J. MOULDER, W. F. STICKLE, P. E. SOBOL and K. D. BOMBEN, "Handbook of X-ray Photoelectron Spectroscopy" (Perkin-Elmer Corporation, 1992) p. 25.
14. J. H. SCOFIELD, *J. Elect. Spectrosc. Related Phenomena* **8** (1976) 329.
15. C. LEA and J. BALL, *Applications of Surf. Sci*. **17** (1984) 344.
16. S. LOPEZ, J. P. PETIT, H. M. DUNLOP, J. R. BUTRUILLE and G. TOURILLON, *J. Electrochem. Soc*. **145**(3) (1998) 823.
17. F. CORDIER and E. OLLIVIER, *Surf. Interface Anal*. **23** (1995) 601.
18. N. A. THORNE, P. THUERY, A. FRICHET, P. GIMENEZ and A. SARTRE, *ibid.* **16** (1990) 236.
19. M. PIJOLAT, V. CHIAVANA and R. LALANZE, *Appl. Surf. Sci*. **31** (1988) 179.
20. M. S. HUNTER and P. FOWLE, *J. Electochem. Soc*. **103** (1956) 482.
21. P. E. DOHERTY and R. S. DAVIS, *J. Appl. Phys*. **34** (1963) 619.
22. A. J. BROCK and M. A. HEINE, *J. Electrochem. Soc*. **119** (1972) 1124.
23. A. KIMURA, M. SHIBATA, K. KONDOH, Y. TAKADA, M. KATAYAMA, T. KANIE and H. TAKADA, *Appl. Phys. Lett*. **70**(26) (1997) 3615.
24. P. L. J. GUNTER, H. J. BORG and J. NIEMANT-SVERDRIET, *J. Vac. Sci. Technol*. **A10**(4) (1992) 2846.
25. T. L. BARR, *ibid.* **14** (1977) 660.
26. F. DEGREVE and J. M. LANG, *Proceedings of Mat. Res. Soc. Symp*. **48** (1985) p. 241.
27. S. SCOTTO, V. ZWILLING, E. DARQUE-CERETTI and M. AUCOUTURIER, Revue de Métallurgie, n° hors série (1996) 173.
28. S. SUGUNAN and B. JACOB, *Indian J. Eng. Mat. Sci*. **4** (1997) 120.
29. M. POURBAIX, in "Atlas d'Équilibres Électrochimiques à 25 °C," edited by Gauthiers (Villars and Cie, Paris, 1963), pp. 141, 172.
30. M. CASAMASSIMA, in "Caractérisation des propriétés acide/base des surfaces d'oxydes d'aluminium et de silicium en vue de la compréhension des mécanismes d'adhésion avec un mastic silicone," Thesis, ENSMP, 1991.
31. T. S. SUN, J. M. CHEN, J. D. VENABLES and R. HOPPING, *Appl. Surf. Sci*. **1** (1978) 202.
32. A. STRALIN and T. HJERTBERG, *ibid*. **741** (1994) 263.
33. G. M. SCAMANS and A. S. REHAL, *J. Mat. Sci*. **14** (1979) 2459.
34. B. R. BAKER and J. D. BALSER, *Aluminum* **3** (1976) 197.

Received 17 June 1998
and accepted 31 March 1999